Rotational Diffusion of Acetylcholine Receptors on Cultured Rat Myotubes

Marisela Velez,* Kate F. Barald,‡ and Daniel Axelrod*§

*Biophysics Research Division, and §Department of Physics, University of Michigan, Ann Arbor, Michigan 48109; and ‡Department of Cell Biology and Anatomy, University of Michigan School of Medicine, Ann Arbor, Michigan 48109

Abstract. The rotational mobility of acetylcholine receptors (AChR) in the plasma membrane of living rat myotubes in culture is measured in this study by polarized fluorescence recovery after photobleaching (PFRAP). These AChR are known to exist in two distinct classes, evident by labeling with rhodamine α-bungarotoxin; clustered AChR that are aggregated in a pattern of highly concentrated speckles and streaks, with each cluster occupying an area of $\sim$1,000 μm^2; and nonclustered AChR that appear as diffuse labeling. PFRAP results reported here show that: (*a*) most clustered AChR ($\sim$86%) are rotationally immobile within a time scale of at least several seconds; and (*b*) most nonclustered AChR ($\sim$76%) are rotationally mobile with characteristic times ranging from <50 ms to 0.1 s. External cross-linking with the tetravalent lectin concanavalin A immobilizes many nonclustered AChR. PFRAP experiments in the presence of carbachol or cytochalasin D show that the restraints to rotational motion in clusters are remarkably immune to treatments that disperse clusters or disrupt cytoplasmic actin. The experiments also demonstrate the feasibility of using PFRAP to measure rotational diffusion on selected microscopic areas of living nondeoxygenated cells labeled with standard fluorescence probes over a very wide range of time scales, and they also indicate what technical improvements would make PFRAP even more practicable.

During development, acetylcholine receptors (AChRs)[1] on the surface of embryonic myotubes undergo a reorganization (Schuetze and Role, 1987; Frank and Fischbach, 1979). At first they are evenly distributed over the myotube surface and then, upon formation of the synapse, they became highly concentrated at the region of nerve-muscle contact. In aneural primary cultures of rat myotubes, the AChR are also present in two distinct populations (Fig. 1): densely clustered receptors (endogenous clusters), which are located mainly in regions of contact between the myotube and the culture dish; and nonclustered diffusely distributed receptors, which are present all along the surface of the myotubes (Axelrod et al., 1976).

There is evidence that at least two different mechanisms participate in the aggregation process: (*a*) lateral redistribution in the plasma membrane of AChRs from the preexisting pool on the surface (Anderson and Cohen, 1977; Stya and Axelrod, 1983; Peng and Poo, 1986; Peng et al., 1989); and (*b*) spatially localized insertion of new receptors from a cytoplasmic pool concentrated at the regions of preferential AChR synthesis near nuclei on aneural cultured myotubes (Pavlath et al., 1989; Harris et al., 1989) or near synapses in vivo (Kuromi, 1987). The cytoskeleton could be involved in either mechanism by: (*a*) actively translocating previously nonclustered AChR into a cluster; (*b*) trapping passively diffusing AChR at a cluster or stabilizing a preexisting cluster (Heuser and Saltpeter, 1979; Hirokawa and Heuser, 1982; Peng, 1983; Bloch and Hall, 1983; Sealock et al., 1984), or (*c*) trapping and localizing myonuclei that produce the AChR message and subsequently, the AChR subunit proteins themselves (Englander and Rubin, 1987).

One of our long-range objectives is to explore the relationship between AChR clustering and cytoskeletal proteins through the study of dynamic properties of the AChR in the plasma membrane. Dynamic properties include both lateral and rotational mobilities, which are usually interpreted as diffusion. Rotational motion measurements provide a different and complimentary type of information to lateral diffusion measurements. Rotational diffusion reflects a short range interaction and, at least according to hydrodynamic theories based on simplified models, it is more sensitive to changes in size and shape of the rotating molecules (Cherry, 1979; Saffman and Delbruck, 1975). In living membranes, other circumstances could completely decouple rotational and lateral behaviors. For example, certain membrane protein molecules might be free to rotate, but lateral motion might be retarded by a tether, anchor, or barrier. At an opposite extreme, free rotation might be inhibited by cross-linking

Dr. Velez's present address is Instituto Roca-Solano, Consejo Superior de Investigaciones Cientificas (CSIC), Serrano 119, Madrid, Spain.

1. *Abbreviations used in this paper*: AChR, acetylcholine receptor; BGT, unlabeled α-bungarotoxin; PFRAP, polarized fluorescence recovery after photobleaching; RBGT, tetramethylrhodamine α-bungarotoxin.

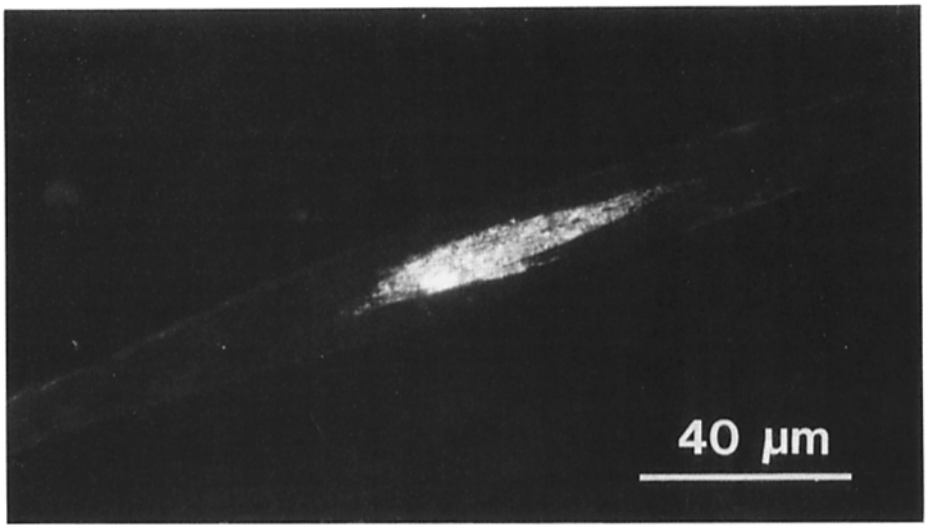

Figure 1. AChR cluster on rat myotube in primary culture, at approximately day 7. The AChR is visualized in epi-illumination by tetramethylrhodamine α-bungarotoxin (Molecular Probes Inc.). The nonclustered AChR are also visible as a diffuse fluorescence particularly prominent along the edges due to tangential viewing. The microscope objective used was a 40× water immersion, 0.75 NA (Zeiss), and the illumination source was a greatly defocused argon laser beam at λ = 514 nm.

but lateral motion enhanced by nondiffusive actively driven jumps. A comparison of rotational and lateral mobility measurements on the same protein in living cell membranes should help distinguish among these and other possibilities.

Coefficients of lateral diffusion have been measured for many membrane proteins in living cells (including the AChR in rat myotube systems) and in lipid bilayer systems using a variety of techniques, particularly fluorescence photobleaching after recovery (FRAP, also called FPR) (Axelrod et al., 1976; Cherry, 1979; Edidin, 1987). FRAP generally measures mobility on distance scales of >1 μm.

Rotational diffusion coefficients (around an axis perpendicular to the membrane) has most commonly been measured (mainly in nonintact cell membrane systems) by time-resolved phosphorescence anisotropy decay (Gonzalez-Rodriguez and Acuna, 1987; Edidin, 1987; Nigg and Cherry, 1980; Lo et al., 1980; Bartholdi et al., 1981) and by polarized fluorescence depletion (Johnson and Garland, 1982; Yoshida and Barisas, 1986). Although these techniques are useful and feasible in many applications, they have two potential limitations for use in living systems: they rely on the excited triplet state lifetime of luminescent probes, which imposes an upper limit of a few milliseconds on the measurement of slower rotational motions; and to achieve that lifetime, they require deoxygenation of the sample, which for an extended duration can be incompatible with the viability of living cells.

In this paper our approach is to measure the Brownian rotational mobility of both clustered and nonclustered AChR on the surface of aneural rat myotubes in living cultures. Rotational diffusion of AChR in membrane preparations has previously been studied in membrane isolates by phosphorescence anisotropy (Lo et al., 1980; Bartholdi et al., 1981); and by spin label electron paramagnetic resonance (Rousselet et al., 1982). For investigating living cells in culture, we use a newer technique, polarized fluorescence recovery after photobleaching (PFRAP), which has been theoretically developed with some generality and tested and verified in model systems (Velez and Axelrod, 1988). PFRAP is somewhat similar to polarized fluorescence depletion except that it is applicable to any time scale, from microseconds to seconds, and does not require deoxygenation.

The main biological goal here is to compare the rotational diffusional behavior of AChR in its various aggregational states on the myotube surface, both before and after application of cluster disaggregating agents. A secondary goal is to explore and demonstrate the feasibility of measuring rotational diffusion on selected microscopic portions of living cultured cells.

Theory

In PFRAP, the initially isotropic distribution of fluorophore orientations (as defined by the directions of the transition dipole moments) is illuminated with polarized light, therefore exciting selectively those fluorophore dipoles oriented with a significant component parallel to the direction of polarization of the incident light. A brief intense pulse of light (of the same or perpendicular polarization) then bleaches the observed fluorophores, thereby inducing an anisotropic orientational distribution of unbleached fluorophore. Rotational diffusion gradually relaxes the anisotropic distribution back toward an isotropic distribution. This relaxation is monitored by postbleach excitation with an attenuated "probe" beam excitation of the same polarization as the prebleach excitation. The resulting time-dependent postbleach fluorescence recovery reflects the characteristic time of the rotational motion of the fluorophores (Fig. 2).

The laser illumination in PFRAP need not be sharply focused; defocusing will lengthen the characteristic time for a recovery due to translation diffusion while not affecting that due to rotational diffusion. With the spot size we use (radius 1.6 μm) and the known translational diffusion coefficient for mobile AChR ($\sim 1 \times 10^{-10}$/s), the translational diffusion time is about three orders of magnitude longer than the longest time scale we use (75 ms) for rotational diffusion measurements, and therefore lateral diffusion should not distort our PFRAP results.

At the fast time scales over which rotational motion can take place (tens or hundreds of microseconds), there is a partial fluorescence recovery independent of molecular orientation or position that tends to obscure rotational effects. This "reversible bleaching" effect, observed even in aerobic samples, was not previously observed at the longer time scales

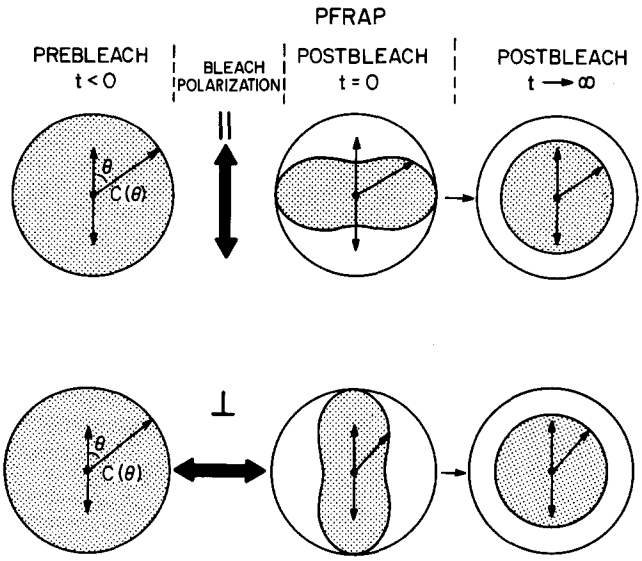

Figure 2. Schematic view of the orientational distribution of unbleached fluorophore before and after bleaching in PFRAP. The radial distance of the edge of the stipled regions from the centers is proportional to the unbleached concentration at the angle θ, measured relative to the polarization direction of the probe illumination (shown as vertical here). The experiment is performed alternately with the bleach polarization in each of the two directions shown, parallel and perpendicular. In principal, the postbleach fluorescence excited by the probe beam should monotonically increase in the parallel mode and decrease in the perpendicular mode. Due to orientation-independent reversible photobleaching, the actual fluorescence recovery is monotonically increasing in both modes (Velez and Axelrod, 1988).

used in standard FRAP for the measurement of lateral motion, and its molecular photophysics remain unclear. However, the increase of reversible bleaching upon depletion of oxygen (Scalettar et al., 1990) and its time scale suggest a bleached-induced population of the triplet state that depletes the fluorophores' ground state population and decays with time after the bleach pulse. Given the independence of reversible bleaching from orientations or polarizations, it is possible to extract the desired information on rotational motion of the molecules simply by running the experiment alternately with a bleaching ("pump") pulse polarized either parallel (subscript $\parallel$) or perpendicular (subscript $\perp$) to its polarization direction during the observation (probe) phase (Velez and Axelrod, 1988).

The "raw" data is the intensity of the prebleach ($t < 0$) fluorescence $F_{\parallel,\perp}(-)$ and the postbleach ($t > 0$) fluorescence $F_{\parallel,\perp}(t)$ for each bleaching polarization $\parallel$ and $\perp$. We define:

$$\Delta F_{\parallel,\perp}(t) \equiv F_{\parallel,\perp}(-) - F_{\parallel,\perp}(t). \quad (1)$$

We also define a "bleaching anisotropy ratio":

$$r_b(t) \equiv \frac{\Delta F_\parallel(t) - \Delta F_\perp(t)}{\Delta F_\parallel(t) + 2\,\Delta F_\perp(t)}. \quad (2)$$

In principle, the ratio $r_b(t)$ cancels out the effects of reversible bleaching recovery, leaving a time-dependent variable which is independent of the state of sample aerobicity and excited state lifetimes and which preserves the dependence on rotational diffusion. Ratio $r_b(t)$, in the PFRAP "pump-and-probe" technique, appears analogous to the anisotropy ratio $r \equiv (F_\parallel - F_\perp)/(F_\parallel + 2F_\perp)$ commonly used in time-resolved polarized luminescence decay "pump-only" techniques, but its mathematical properties are somewhat different.

The theory of PFRAP (Velez and Axelrod, 1988) offers exact explicit forms for $r_b(t)$ in terms of the rotational diffusion coefficient for arbitrary bleaching depth and for fluorophores undergoing restricted fast wobbling at the covalent bond of attachment. The expression for $r_b(t)$ used here, for rotational diffusion in two dimensions about a normal to the membrane plane is

$$r_b(t) = \frac{2b\, e^{-4D_r t}}{3a + b\, e^{-4D_r t} - 3c\, e^{-16D_r t}}, \quad (3)$$

where D_r is the rotational diffusion coefficient of the rotating molecule. Factors a, b, and c have exact but complicated forms involving the wobble angles of the fluorophore, the angle between the absorption and emission dipoles, and the bleaching depth. The amplitude of the anisotropy $r_b(t)$ always remains positive and monotonically decreasing in time, regardless of interdipole angles, fast wobbling amplitude, and bleaching depth. For the shallow bleaches used here (less than ~40%), $b/a \cong 0.5$ and $c/b << 1$, so under these conditions, the shape of $r_b(t)$ can be approximated as the single exponential appearing in the numerator (since the faster decaying, higher order terms in an expansion of Eq. 3 will have an amplitude of no more than ~16% of the first term). Multiexponential fits then represent heterogeneity in the rotational mobilities present in the sample.

Materials and Methods

Cell Culture

Fetal rat myotube primary cell suspensions from 18–20-d-old rat embryos were prepared as previously described (Axelrod et al., 1976; Barald et al., 1987). The medium consisted of 90% DME, 10% FCS, and 0.6 μg/ml tetrodotoxin (TTX; Sigma Chemical Co., St. Louis, MO). At plating time, a 2-ml aliquot containing 3.5×10^5 cells/ml in suspension was added to a 35-mm tissue culture dish containing a clean and sterile (but reused) 25-mm diameter fused silica coverslip (Heraseus-Amersil, Inc., Sayreville, NJ). Medium was replaced on day 4 with fresh medium containing 20 μM cytosine arabinoside, added to reduce the growth of nonmuscle cells. Cells were usually examined 6–8 d after plating, when large clusters of AChR had formed in the substrate-apposed membranes of the myotubes. At this stage, myotubes were ~400 μm long, and ranged in width from 15–40 μm. AChR clusters usually formed at the widest segments of myotubes. Before measuring rotational mobility of AChR, the medium was removed and replaced with a solution of fluorescent tetramethylrhodamine α-bungarotoxin (RBGT) (Molecular Probes Inc., Eugene, OR) at ~10^{-7} M in PBS for ~20–30 min at 22°C. RBGT binding is irreversible on the time scale of our experiments. After several washings, the fused quartz coverslip was mounted, immersed in PBS containing TTX, in a sealed chamber (Bellco Glass, Inc., Vineland, NJ). For preparing cells for measurement of background fluorescence, the same procedure was followed except that the cultures were first exposed to unlabeled α-bungarotoxin at 10^{-7} M for 30 min at 22°C before exposure to RBGT.

Coverslips made of fused silica (99% pure SiO_2) (sometimes called "quartz" although it is a glass and not a crystal) were used to avoid the strong standard microscope coverslip glass autofluorescence, which has a decay time of a few hundred microseconds, and which would severely interfere with luminescence measurements on that time scale.

Binding RBGT to Fused Silica Slides

RBGT was covalently attached to succinylated fused silica microscope slides (Heraseus-Amersil Inc.). The succinylation procedure used was based on that described by Jacobson et al. (1978) for covalently attaching

polylysine to glass beads via an organosilane reaction. As adapted for use in this laboratory, the procedure is performed with slides instead of beads and with RBGT instead of polylysine.

Concanavalin A Treatment

Cells were labeled with RBGT as described above. The cultures were then washed thoroughly with PBS. Concanavalin A (Sigma Chemical Co.) was then added to the buffer to reach a final concentration of 0.1 mg/ml. The cells were incubated in this solution for 30 min.

Cytochalasin D Treatment

Cytochalasin D (Sigma Chemical Co.) was dissolved in dimethylsulfoxide at 1 mg/ml concentration. It was then diluted in PBS to a 20 μg/ml concentration and that solution was added to the medium in the tissue culture dish containing the cells to reach a final concentration of 0.2 μg/ml (Connolly, 1984). The plates were then returned to the incubator for 3 h before labeling with RBGT and obtaining measurements.

Carbachol Treatment

Culture medium was removed and replaced with a 10^{-7} M solution of RBGT for ~1 h at 37°C. The cultures were washed several times before adding back the medium, to which 10^{-4} M carbachol (Sigma Chemical Co.) had been added. Cultures were then placed in the incubator for 4–6 h before PFRAP measurements. During the PFRAP experiments, the phosphate buffer containing TTX in the sealed chamber (Bellco Glass, Inc.) also contained 10^{-4} M carbachol.

To quantify the cluster dissaggregating effect of carbachol, we counted the number of RBGT-marked AChR clusters per unit myotube surface area in photographic enlargements (taken with a Nikon 20× glycerol, 0.8 NA objective, and Kodak TMAX P3200 film) of carbachol-treated and control cells. The myotube surface area, in arbitrary units, was assayed by cutting out the myotube images and physically weighing the cut print paper on an analytical balance. Three separate values for each experimental condition were obtained on different days.

Optics and Electronics

The optical system is described in Fig. 3. Because of the short time scale of some PFRAP experiments, signal/noise ratio is limited by shot noise, and it is thereby desirable to gather as many photons as possible. In addition, a significant bleaching depth must be achieved with a microsecond-duration bleaching pulse. Both goals are approached by using a laser with a significantly higher power than those used in conventional lateral diffusion FPR. We use a 15 W CW argon laser (Coherent Innova Series 20; Coherent Inc., Palo Alto, CA) at λ = 514.5 nm.

The actual laser power (P) incident upon the sample was adjusted by neutral density filters for the different bleaching durations (t_b) to ensure approximate constancy of the bleach depth, as follows: (t_b = 10 μs, P = 300 mW); (t_b = 500 μs, P = 6 mW); (t_b = 1,500 μs, P = 2 mW).

The heating caused by a bleaching flash can limit the usable range of incident laser powers and focused radii. The temperature increase due to light absorption by the fluorophore can be calculated (Velez and Axelrod, 1988). For the worst case, with P = 300 mW at t_b = 10 μs and e^{-2} beam radius = 1.6 μm, and with the concentration of rhodamine in a cluster = 5×10^3 fluorophores/μm^2, we calculate (Velez and Axelrod, 1988) that the consequent temperature rise by the termination of the bleaching pulse is ~3.6°C. The lower power bleaching flashes used at longer bleach durations produce much smaller temperature increases.

Computer control of the electroptical elements as well as the photon counting has been described previously (Velez and Axelrod, 1988). Extensive signal averaging of PFRAP curves was required for good signal/noise ratios. Rather than using repeated bleaching flashes in the same spot and relying on translational diffusion to restore the fluorescence to its prebleach level, we moved the sample on the microscope stage in 2-μm jumps to a fresh unbleached spot before each bleaching flash in a rectangular array of user-specified dimensions, by means of computer-controlled microstepper motors. The repetition rate was 10 per second, so that sufficient dead time was left for damping of jump-induced vibrations.

Data Acquisition

The data (photon counts per sample bin vs. time) were signal averaged over

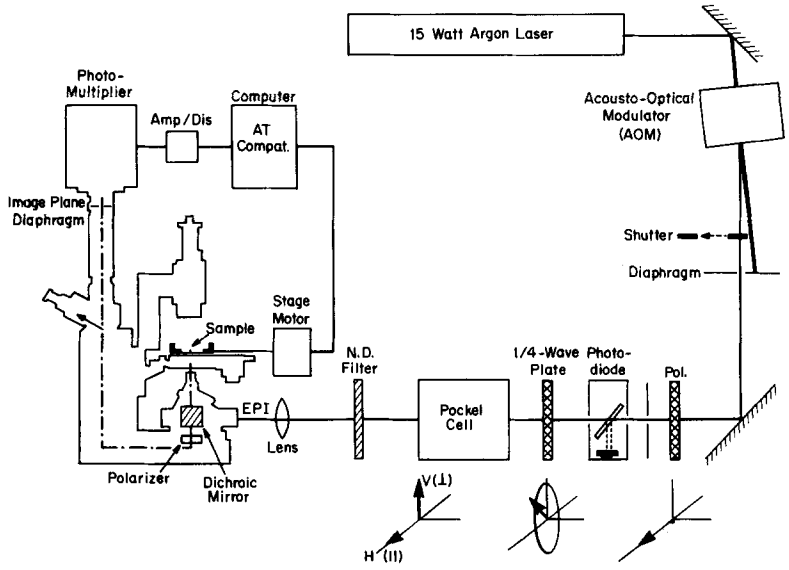

Figure 3. The laser beam intensity is controlled by an acousto-optic modulator (AOM; IntraAction Corp., Bellwood, IL), the first-order diffraction throughput of which supplies both the bleaching and probe intensities. The AOM was adjusted so that the ratio of these intensities was ~2,000:1. The beam then passes through a crystal polarizer oriented horizontally to correct the slight depolarizing effect of the AOM. The beam then passes through a 1/4-wave plate (for λ = 514.5 nm) and through a transverse field Pockels cell (Lasermetrics Inc., Englewood, NJ). The applied voltages to the Pockels cell are adjusted such that the output polarization is vertical during a transient pulse (during bleaching in the ⊥ mode only) and horizontal at all other times. The beam passes through a simple converging lens immediately before the entrance field diaphragm of a standard epifluorescence microscope (Leitz Diavert) illuminator. The converging lens position can be adjusted by a x, y, z precision translator to set the lateral position and to adjust the spot size at the field diaphragm plane (and correspondingly at the sample plane). The spot was always centered, but it was slightly defocused to avoid overheating and overbleaching the sample while retaining a high total power. The microscope itself was equipped with a 40×, 0.75 NA water immersion achromat objective (Zeiss) and dichroic/barrier filter combinations specially optimized for the λ = 514 nm line of the source. The illumination spot on the sample had a $1/e^2$ radius of 1.6 μm. After passing through the barrier filter, the fluorescence was repolarized by a film disk (Polaroid), always oriented parallel to the excitation polarization direction of the probe beam. The fluorescence image was delimited by an adjustable image plane diaphragm (part of the Leitz MPV-1 photometer unit), positioned to pass the light from most of the central portion of the illuminated spot. The fluorescence was detected by a high cathode sensitivity, thermoelectrically-cooled photomultiplier (C31034A; RCA Electro-Optics). A standard Merzhauser microscope stage was custom modified so that its x and y direction ball slides were driven by high-pitch precision lead screws connected to two computer-driven (and optionally, joystick-driven) microstepping stepper motors (Compumotor Div., Rohnert Park, CA).

many tens to hundreds of thousands of individual fluorescence recovery curves. These recovery curves were gathered in groups. Only regions of the myotube that were free of debris were sampled. Since endogenous AChR clusters appear almost exclusively on the bottom (substrate-facing) surface of the myotubes, all PFRAP runs (at both clustered and nonclustered regions) were performed on the bottom surface. A clustered or a nonclustered region was located by visual inspection of broad area epi-illumination fluorescence, and a group of recoveries was then recorded from sequentially bleached spots positioned in the largest rectangular array that could be completely imbedded in the region, all under automated computer control. (Typically, a clustered region rectangle was ~30 × 10 μm, and a nonclustered region rectangle was ~120 × 15 μm). Then a new region was visually selected and the automated process repeated, with the recoveries signal averaged on-line with those of the previous region of interest. The number of individual bleach/recoveries attainable in each group varied from several tens (from a single cluster) to several hundred (from a single contiguous nonclustered region). The clarity of focus during each brief automatic scan sequence was assured by a visual check after each sequence; even if some random unseen defocusing did occur due to irregularities in the bottom surface of myotubes, signal-averaged PFRAP anisotropy results should be rather insensitive to it.

The first 50 sample bins detect the fluorescence (always excited with polarization parallel to the emission polarizer direction). The bleaching pulse (alternately polarized in the parallel and perpendicular directions) generally has the same duration as a single sample bin, and the next 150 sample bins after the bleaching pulse observe the postbleach fluorescence recovery (always excited in the parallel polarization direction). The automatic alternation between parallel and perpendicular polarization at immediately adjacent bleaching spots minimizes the effect of biological variabilities over larger distances on the myotube surface.

It is important that the relative intensities of the parallel and perpendicular bleach pulses at the sample are known, and if they are not equal, the sample data must be corrected for the difference. The relative intensities were measured by performing comparable PFRAP experiments on samples that exhibited rapid molecular tumbling on the time scale of the myotube experiments; i.e., an aqueous solution of RBGT sandwiched between fused silica coverslips. In such samples, equal bleach intensities in the two polarizations should give rise to $r_b(t) = 0$ for all t. Conversely, corrections for nonequal bleach intensities can be calculated, if necessary, from a nonzero r_b measured on such a sample. We found that r_b was close to zero on rapidly tumbling samples without further correction.

The maximum anisotropy value, $r_b(0)$, decreased more rapidly with increasing bleach depth than predicted by theory. This is probably due to rhodamine groups in different local environments exhibiting a wide range of bleachabilities. Therefore we limited the bleach in all cases to ~30% of the initial fluorescence.

The sample bin durations that were used to analyze the different rotating components were 10, 500, and 1,500 μs. To improve the signal/noise in each bin, we combined five neighboring bins into one, which is equivalent to having done the experiments with sample bin durations of 50, 2,500, and 7,500 μs. These correspond to postbleach recovery durations of 1.5, 75, and 225 ms, respectively. It is always this "compressed" data that was analyzed by fitting as explained below.

Because the cell's autofluorescence can contribute a substantial portion (about one-third) of the fluorescence in areas with nonclustered RBGT-AChR, we gathered PFRAP data on myotubes whose AChR had been blocked by an excess of unlabeled α-BGT before exposure to RBGT. A large number of such background runs for each polarization mode (~200,000 for the 50-μs sample time experiments, 30,000 for the 2,500-μs sample time, and ~10,000 for the 7,500-μs sample time) were gathered on the same day on the same culture set as the corresponding RBGT-AChR data and were routinely subtracted from the respective fluorescence data taken on the RBGT-labeled myotubes.

Fitting

The purpose of fitting is to derive D_r from $r_b(t)$ with as few free fitting parameters as possible. We used a nonlinear squares fitting program (Bevington, 1969). The anisotropy $r_b(t)$ to which the data points were fitted was based on Eq. 3, except with two modifications. First, Eq. 3 was made simpler by assuming approximating it as a single exponential for a single D_r, as discussed earlier. Second, Eq. 3 was made more complicated by assuming a heterogeneity of rotational rates in the sample, described by two, rather than one, rotational diffusion coefficients D_{r1} and D_{r2}. The expression used is:

$$r_b(t) = \frac{2b}{3a}\{\alpha_1[exp(-4D_{r1}t) - exp(-4D_{r2}t)] + exp(-4D_{r2}t)\}, \quad (4)$$

where a and b constants are described in the theory section, α_1 is the fraction of fluorophores with D_{r1} and $1 - \alpha_1$ is the fraction with D_{r2}. We allowed four parameters to be fitted: b/a, α_1, D_{r1}, and D_{r2}.

The maximal possible $r_b(t)$, denoted as r_b^{max} appears to be limited largely by the extent of wobbling of the fluorophore (tetramethylrhodamine) on the protein (α-bungarotoxin). Experimentally, r_b^{max} should be determined from PFRAP experiments on an appropriate sample in which the protein itself is known to be immobilized. On such a sample, the measured $r_b(t)$ should be constant in time and equal to r_b^{max}. Then, in any other sample where a significant fraction $(1 - \alpha_s)$ of the fluorophore is very rapidly mobile (on a time scale shorter than the experimental sample bin duration) and the remaining fraction α_s is either more slowly mobile (on the time scale of a sample bin or longer) or totally immobile, the initial postbleach anisotropy will be somewhat reduced from its maximal possible r_b^{max}. Slowly mobile fraction α_s can be calculated from a comparison of the experimentally measured $r_b^{exp}(0)$ with r_b^{max}. Note that the calculation is more complex than taking a simple proportion with respect to r_b^{max} because r_b is itself a ratio. The result is:

$$\alpha_s = \frac{r_b^{exp}(0)\,(1 + 2r_b^{max})}{r_b^{max}\,[1 + 2r_b^{exp}(0)]}. \quad (5)$$

The "slow" fraction α_s includes both slowly mobile and totally immobile fluorophores. To calculate only the fraction of fluorophores α_i that are totally immobile throughout the recovery duration from Eq. 4, simply substitute α_i for α_s and the asymptotic value $r_b^{exp}(\infty)$ for $r_b^{exp}(0)$:

$$\alpha_i = \frac{r_b^{exp}(\infty)\,(1 + 2r_b^{max})}{r_b^{max}\,[1 + 2r_b^{max}(\infty)]}. \quad (6)$$

The uncertainty of each fitted point of $r_b(t)$ was calculated by propagating the shot noise statistical uncertainty of each data point in $F_{\parallel,\perp}(t)$ as guided by Eq. 1. From these uncertainties, the fitting program derived the uncertainties of the fitted parameters.

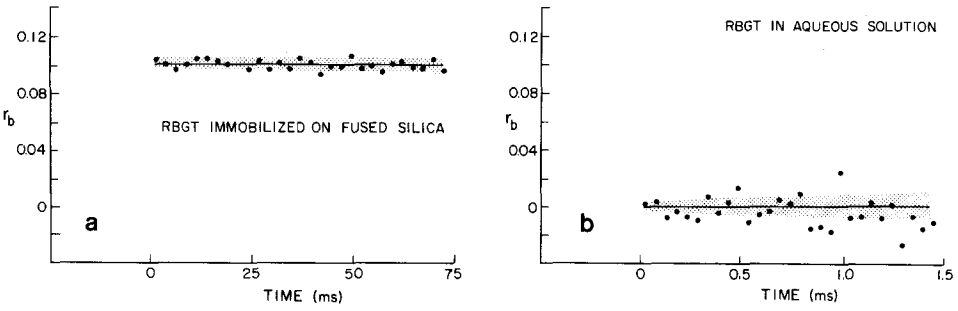

Figure 4. (*a*) Bleaching anisotropy for RBGT immobilized on fused silica. This data is based on ~6,100 signal-averaged bleach/recovery cycles in each polarization mode. (*b*) Bleaching anisotropy for RBGT freely tumbling in HBSS. The data is based on ~133,500 signal-averaged bleach/recovery cycles in each polarization mode. The dots are calculated from the original $F_{\parallel,\perp}(t)$ data (not shown) according to Eqs. 1 and 2; the solid line is a nonlinear least squares fit as described in Materials and Methods; the stippled area represents the uncertainty range arising from shot noise as described in Materials and Methods.

Results

Immobile and Rapidly Mobile RBGT

We measured $r_b(t)$ for both a sample of artificially immobilized RBGT sample (to determine r_b^{max}) and a very rapidly tumbling RBGT sample (to check the equality of the parallel and perpendicular bleach intensities).

The immobile sample is created by covalently binding RBGT to a fused silica slide and bathing it in HBSS. Although RBGT in this preparation may not be completely immobile, it is likely to be at least as immobile as any AChR on myotubes, and the immediate aqueous environment of the rhodamine fluorophore is still preserved. Fig. 4 *a* shows the anisotropy ratio obtained at an intermediate time scale. Note that the anisotropy is positive and nondecaying in time, at a value of $r_b = 0.1 \pm 0.005$. This r_b is lower than the theoretical maximum of 4/7 (Velez and Axelrod, 1988), presumably because of rapid wobbling of the fluorophore on the unlabeled α-bungarotoxin (BGT) or rapidly internal flexing motions in the BGT. We interpret this r_b to be the maximum attainable with immobilized RBGT and denote it as r_b^{max}.

The results for r_b on immobilized RBGT were somewhat variable from preparation to preparation, ranging from as low as 0.085 to as high as 0.12. This variability may reflect actual uncontrolled differences in the amount of multivalency in the binding of RBGT to fused silica. This probably arises from variations in the surface concentration of bound organosilane, the reactivity of which is extremely sensitive to the presence of water.

The very fast rotating sample consists of RBGT dissolved in HBSS. According to hydrodynamic theory, this sample should present a rotational correlation time of ~5 ns, which is much shorter than our PFRAP time scale. Therefore, the immediately postbleach orientational distribution of unbleached fluorophore becomes completely isotropic during the bleach pulse, and very little postbleach anisotropy should be evident, even at our fastest times scales. Fig. 4 *b* shows that this is indeed the case on our fast times scale of 1.5 ms, thereby confirming that the bleach intensities for parallel and perpendicular polarizations are very similar.

On the basis of these results, we expect the anisotropy of any rotating RBGT/AChR on rat myotubes to vary between the extremes of ~0.12 and 0.00.

Clustered vs. Nonclustered AChR

The rotational behaviors of clustered and nonclustered RBGT/AChR were very different from each other and from the immobile and mobile model systems described above. The distinction between clustered and nonclustered regions was apparent at both short and longer time scale PFRAP experiments. A large proportion of the AChR aggregated in large clusters do not show any rotation, and the AChR found in the nonclustered regions show a heterogeneous mixture of components with different rotational rates.

Fig. 5 shows the actual $F_{\parallel,\perp}(t)$ curves for both clustered and nonclustered AChR on the 75-ms time scale, Note that the two polarizations are much more separated in the clustered case, indicating a higher degree of immobilization. Fig. 6 *a* shows the bleaching anisotropies $r_b(t)$ for both clustered and nonclustered AChR on the 75-ms time scale, as derived from the fluorescence intensity data of Fig. 5. Fig.

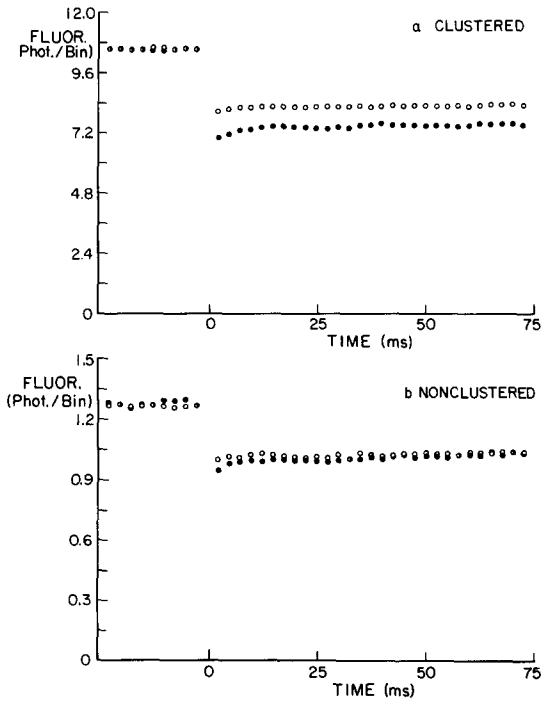

Figure 5. Fluorescence intensities $F_{\parallel,\perp}(t)$ for (*a*) clustered AChR and (*b*) nonclustered AChR, 75-ms time scale. Parallel and perpendicular bleach data points are denoted by closed and open circles, respectively. The ordinate units are the actual average number of photons observed per sample bin per bleach/recovery cycle. The clustered and nonclustered AChR data are based on ~42,000 and 110,200 signal-averaged bleach/recovery cycles, respectively, in each polarization mode.

6 *b* shows the corresponding $r_b(t)$ curves, except at the faster time scale of 1.5 ms.

For clusters, $r_b(t)$ starts at $t = 0$ on the 75-ms curve at a high value of ~0.12. This is as large as the r_b on any of the immobilized RBGT/fused silica samples we have prepared. We therefore conclude that essentially none of the AChR in clustered regions rotationally diffuses in a time shorter than the sample bin duration here, 2.5 ms. Subsequently, $r_b(t)$ declines to an asymptotic value of 0.10 ± 0.004. From Eq. 6 (setting $r_b^{max} = 0.12$), we conclude that ~86% of the clustered receptors are rotationally immobile ($D_r < 0.2$ s^{-1}) and ~14% do rotate slowly with $D_r \cong 30 \pm 14$ s^{-1}. On the shorter recovery duration scale of 1.5 ms, r_b is essentially constant as expected.

For nonclustered regions, the $r_b(t)$ curves of RBGT/AChR obtained with recovery durations of 1.5 and 75 ms show at least four different rotating components: (*a*) one that rotates with a $D_r > 5{,}000$ s^{-1} (corresponding to a time shorter than a few tens of microseconds), bringing $r_b(t)$ down from the 0.12 value assumed for a completely immobile sample to ~0.065; (*b*) a second component that rotates with a D_r of 700 ± 80 s^{-1}; (*c*) a third component that rotates with a D_r of 2.9 ± 0.6 s^{-1}; and (*d*) a fourth rotationally immobile component that prevents $r_b(t)$ from decaying to zero, leaving it at an asymptotic value of 0.02 ± 0.01 s^{-1}.

From the $r_b(0)$ and $r_b(\infty)$ values for each time scale, one can calculate, by means of Eqs. 5 and 6, the fractions of the

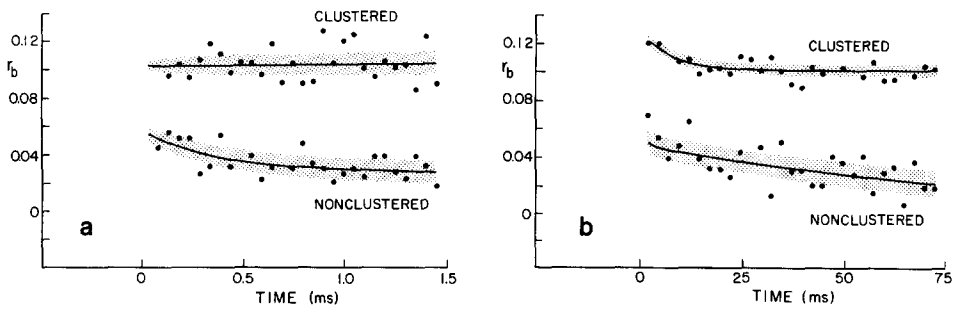

Figure 6. (*a*) Bleaching anisotropy for clustered and nonclustered AChR on myotubes, 75-ms time scale, based on the fluorescence curves displayed in Fig. 5. (*b*) Bleaching anisotropy for clustered and nonclustered AChR on myotubes, 1.5-ms time scale. This curve represents signal averaging of ~623,000 bleach/recoveries for each polarization mode. The notations are the same as in Fig. 4.

different rotational components in nonclustered areas. Table I summarizes these fractions with their D_r values.

We explored even faster time scales (2-μs sample bins), but the results were not conclusive. RBGT shows an anomalous behavior (a positive slope) at short time scales. This anomaly, highly dependent on the local fluorophore environment, was also seen in polarized fluorescence depletion experiments (Yoshida and Barisas, 1986) and was discussed at length by Velez and Axelrod (1988). It obscures any anisotropy decay that occurs at very short time scales. Furthermore, photon shot noise becomes a limiting factor for short sample times. More averaging can always surmount shot noise but the experimental time may become forbidding if most of the time is consumed by visual searching rather than by actual data acquisition. It is likely that this limitation can be overcome by more efficient and automated searching methods.

In the two times scales covered by Fig. 6, *a* and *b*, there is a slight mismatch in the $r_b(0)$. This may be due to a variety of factors, both instrumental and biological. (*a*) We find that the Pockels cell's transmitted light is not absolutely stable over time in intensity and polarization purity. Although the problem is not severe, it adds effective noise to the results. The latest version of the optics achieves more stable rapid polarization switching by use of static crystal polarizers and shutters instead of a Pockels cell. (*b*) Anisotropy $r_b(0)$ is a function of the bleaching depth (Velez and Axelrod, 1988). Although the same bleaching intensity was always used in corresponding experiments on different days, the bleaching depth often varied over a small range, presumably with the level of dissolved oxygen in the buffer. Also, at different bleaching durations (as in Fig. 6, *a* and *b*), the intensity was adjusted to yield a constant bleaching depth, but the constancy was only approximate. (*c*) The subtraction of autofluorescent background, particularly important for the dim nonclustered AChR regions, is a potential source of noise, since the background level varies somewhat among different culture platings and is spatially highly variegated.

Table I.

Component	D_r (s^{-1})	Percent
Fast	≥5,000	31 ± 4
Intermediate	700 ± 80	15 ± 7
Slow	2.9 ± 0.6	30 ± 11
Immobile	≤0.1	24 ± 9

Rotational diffusion coefficients and percentage of total AChR in nonclustered regions on myotubes. The uncertainties are derived from the statistical uncertainty (photon shot noise) of the original data.

(*d*) There may exist an actual biological variability from culture set to set, particularly as a function of cell age, which is known to affect AChR distribution. Despite these potential sources of noise in $r_b(0)$, the internal comparisons of clustered vs. nonclustered AChR in each of Fig. 6, *a* and *b* are valid because, within each panel, data were gathered from the same distinct set of cultures.

Extrinsic Cross-linking of Nonclustered AChR by Con A

To determine if the rotational diffusion of the nonclustered AChR could be inhibited by extrinsic agents, we incubated the cells with the tetravalent lectin Con A after labeling with RBGT. This lectin is known to cross-link the nonclustered receptors and to inhibit their lateral motion (Axelrod et al., 1978). Experiments done at the 75-ms time scale show a very clear increase in $r_b(t)$ of the Con A–treated samples compared with nontreated cells to an almost constant anisotropy value of ~0.075 ± 0.01 (Fig. 7).

Another standard cross-linking treatment, fixation with 5% paraformaldehyde, did not affect the anisotropy decay of the nonclustered receptors. Although this result seems surprising, it is consistent with the observation of Cone (1972), who reported no effect of paraformaldehyde on the rotational diffusion of the membrane protein rhodopsin in retinal rod outer segment membranes.

Disaggregation of Clustered AChR

The molecular mechanism of AChR immobilization in clus-

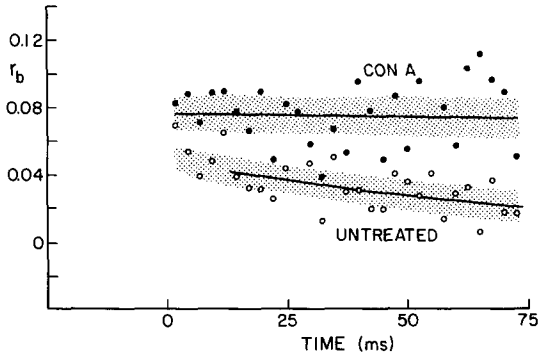

Figure 7. Bleaching anisotropy for nonclustered AChR, Con A–treated vs. untreated, 75-ms time scale. The Con A–treated and untreated curves (the latter being identical to the nonclustered AChR curve of Fig. 6 *a*) represent signal averaging of ~66,200 and 110,200 bleach/recoveries, respectively, in each polarization mode.

ters may be elucidated by treatment with agents that are known to have specific disruptive effects on cells. For myotubes, one such agent is carbachol, a receptor agonist that causes the disappearance of AChR clusters on the surface of living rat myotubes (Bloch, 1986*a*). The mechanism by which carbachol affects the receptor distribution is unknown.

We treated cells with carbachol in a slightly different protocol from the one described by Bloch (1986*a*) to disrupt AChR clusters. In the Bloch experiments, the carbachol treatment preceded the labeling with RBGT. In our case, since we wanted to follow the dynamics of the effects of carbachol, we labeled first with RBGT, then incubated with carbachol, and then performed the PFRAP measurements with carbachol still present in the medium.

Our results on cluster loss agree qualitatively with those of Bloch, who measured the fraction of myotubes with at least one surviving cluster. Our results quantify the actual number of surviving clusters per area of myotube. In three different trials, done on separate days, we observed that the carbachol treated cells presented a 79, 67, and 43% loss in number of clusters per unit surface area of myotube compared to the untreated cells.

The cluster-dispersing effect of carbachol is only seen at 37°C, so PFRAP experiments were carried out at 37°C by heating the sample at the microscope stage with a thermostatically controlled heated air blower.

PFRAP experiments showed only a slight and marginally significant difference between the bleaching anisotropies for carbachol-treated and untreated clusters. Both yielded nondecaying $r_b(t)$ curves on a 225-ms time scale. For carbachol-treated clusters, $r_b = 0.095 \pm 0.01$ (based on ~14,800 bleach/recoveries); and for untreated clusters, $r_b = 0.085 \pm 0.01$ (based on ~9,100 bleach/recoveries), both at 37°C rather than the 22°C of all other experiments. These measurements were done on the clusters that were still fairly well structured, with a typical visible pattern of semi-aligned speckles and punctate spots. Experiments carried out at room temperature (22°C) showed no difference in anisotropy value for treated and untreated cells.

Another disaggregating agent we used was cytochalasin D, which is known to cause selective depolymerization of a class of nonmyofibrillar actin filaments on chick myotubes, and which causes a loss of AChR clusters (Connolly, 1984; Connolly and Graham, 1985). Treatment of cells with cytochalasin D did not affect the rotational mobility of clustered receptors as measured by PFRAP at 22°C. No direct assessment of the effect of the treatment on cluster loss was performed because even after only a 3-h treatment the myotubes had noticeably changed their morphological appearance. Most of them had become rounded and partially detached from the substratum. In spite of these dramatic morphological changes, PFRAP experiments could still be performed because a large number of clusters remained, mainly in the small areas of contact between the "myoballs" and the culture dish.

Discussion

The rotational motion of the AChR in its two aggregational states on the plasma membrane of rat cultured myotubes, clustered and nonclustered, are clearly different: most clustered receptors are rotationally immobile ($D_r < 0.2\ s^{-1}$), whereas most nonclustered receptors are rotationally mobile with rates ranging from $D_r \cong 3\ s^{-1}$ to $D_r > 5{,}000\ s^{-1}$. Nevertheless, a small fraction (16%) of AChR in clusters are slowly mobile ($D_r \cong 30\ s^{-1}$) and a minority (25%) of AChR in nonclustered regions are immobile ($D_r < 0.2\ s^{-1}$).

The detection by PFRAP of a slow ($D_r = 3$–$700\ s^{-1}$) but nonzero rotational rate on myotubes extends previous phosphorescence anisotropy results for AChR found in other biological systems. Earlier measurements of the rotational motion of AChR (Lo et al., 1980; Bartholdi et al., 1981) in *Torpedo* electric organ found the receptors to be immobile, in the unmodified membrane, for at least the 1-ms time scale of the experiment. But in membranes depleted of peripheral proteins or subjected to chemical modifications of the thiol groups, a much faster rotation of the monomeric receptor ($D_r = 4$–$10 \times 10^4\ s^{-1}$) was measured. In those experiments on AChR, as well as in other phosphorescence decay studies in which rotational immobility of a membrane protein was detected (Peters and Cherry, 1982; Brown, 1972; Zidovetzki et al., 1981; Richter et al., 1979; Edidin, 1987; Cherry, 1979; Gonzalez-Rodriguez and Acuna, 1987), the apparently immobile protein actually may have been rotating on a time scale too long to be detected by techniques limited by the triplet state lifetime.

Although it is not possible to draw precise molecular models based only on the amplitude of rotational (or lateral) diffusion coefficients, certain conclusions can be drawn from a comparison of rotational and lateral motion in the same membrane region from the viewpoint of certain simplified membrane models.

Free Diffusion of AChR Aggregates

The simplest model is that of Saffman and Delbruck (1975), which describes free diffusion of cylindrical proteins in a lipid sandwich of uniform viscosity between water layers. Given a fixed membrane viscosity $\eta = 1$ p and a membrane thickness $h = 7$ nm, one can calculate the cross-sectional area of a cylinder that would account for each of our observed D_r values, by using their rotational diffusion equation:

$$\pi a^2 = kT\,(4D_r\,\eta h)^{-1}. \tag{7}$$

This cross-sectional area can then be transformed roughly into a corresponding maximum number of AChR aggregated into a cylindrical oligomer, assuming each AChR monomer has a cross-sectional area of ~130 nm² (Brisson and Unwin, 1985).

This approach leads us to conclude that, under the cylindrical oligomer assumption, the fastest rotating component (that found with $D_r > 5{,}000\ s^{-1}$ in nonclustered areas) cannot be larger than ≅16 monomeric receptors. If oligomers are not as tightly packed (e.g., the case in which individual monomeric cylinders are connected by rigid cross-links such that lipid can flow through the oligomer), then the upper limit for oligomeric size that could account for the fastest component would be even smaller than 16.

Our PFRAP results, then, are clearly consistent with a model in which the fastest component consists of free AChR monomers rotating freely or almost freely in the membrane. On the other hand, even the fastest lateral diffusion of nonclustered AChR (Axelrod et al., 1976) is at least 10–100 times slower than predicted for free lateral diffusion. This

retardation of lateral diffusion, typical of many membrane proteins (Jacobson et al., 1987; Wolf, 1986; Petersen, 1984), suggests that there must be physical barriers to long-range diffusion whereas short-range motion measured by rotation can remain free (Schlessinger, 1983; Cherry, 1979).

The second measured rotating component in nonclustered areas, with $D_r = 700 \pm 80\ s^{-1}$, could contain up to ≅120 monomeric receptors according to the Saffman and Delbruck model. The third component in nonclustered areas, with $D_r = 2.9 \pm 0.6\ s^{-1}$, could contain up to 10,000 monomeric AChR in a microaggregate. However, an aggregate that size would have a dimension of about a micron, which could be easily resolved by a light microscope. Nonclustered regions on RBGT-labeled cultured rat myotubes do show tiny aggregates, but they are not as bright as would be expected for microaggregates densely packed with such a large number of monomeric receptors. It is also possible that the rotating aggregates contain other proteins than AChR. If such nonlabeled proteins contribute to the aggregates, the aggregates might not be as bright as those containing only labeled receptors.

For the immobile AChR, which are a minority (~20%) in nonclustered regions, self-aggregation would require unreasonably large oligomers of ~500,000 receptors, which for some reason cannot be seen. To account for the presence of nonclustered but yet immobile AChR, it seems more likely that there are rotational constraints other than a Saffman-Delbruck viscous drag on huge self-aggregates. On the other hand, clustered AChR, which are both rotationally immobile and quite obviously concentrated in the membrane, could be immobilized both laterally and rotationally by self-aggregation on a very large scale.

Self-aggregation in nonclustered areas is apparently induced extrinsically by tetravalent Con A, which can bind to AChR directly. Con A affects both the fast and intermediate range diffusion; this is clear, respectively, from the increase of $r_b(0)$ relative to untreated cells and the subsequent constancy of the $r_b(t) = 0.075 \pm 0.001$. The Con A experiments were intended as a control, to show that nonclustered AChR on untreated cells exhibited a mobility that could be partly abolished. The mechanism of the Con A–induced immobilization cannot be concluded from just this one result. The simplest view is that a superaggregate of mobile AChR is formed by cross-links with Con A. According to the Saffman-Delbruck assumptions of Eq. 7, such as aggregate must involve at least 30,000 monomeric receptors. It is also possible that some mobile AChR are simply cross-linked to the minority of already immobile AChR present in nonclustered regions in cells that were not treated with Con A or to other already immobile Con A receptors on the surface of the membrane.

Stollberg and Fraser (1988) have recently shown that some sort of surface interactions are responsible for a marked tendency of AChR to self-aggregate. The lateral and rotational diffusion of self-aggregated AChR can be examined in a reconstituted planar membrane system by FRAP and PFRAP; our experiments are proceeding in that direction.

Cytoplasmic and Exoplasmic Attachments

Another model (other than Saffman-Delbruck) to explain the pattern and dynamics of myotube AChR is to postulate their connection with cytoplasmic filaments. There is evidence for the existence of cytoskeletal and extracellular matrix structures during the formation of aggregates (Olek et al., 1986) and of cytoskeletal protein specializations adjacent to the AChR clusters (Bloch, 1986*b*; Bloch et al., 1989 and references therein). The 43-kD protein, an actin-binding protein found to codistribute with AChR, is a good candidate as a cytoplasmic linker for AChR. It is known to be in close contact with the AChR in clustered regions (Peng and Froehner, 1985). Furthermore, Lo et al. (1980) and Bartholdi et al. (1981) showed that high pH, which leads to depletion of 43-kD proteins in *Torpedo* membrane fragments, allowed previously immobile AChR to rotate.

The predominant rotational immobility of AChR in clusters argues against the otherwise reasonable hypothesis (e.g., Koppel et al., 1981) that lateral barriers or tethers inhibit the receptor from any long range (≅1 μm) lateral motion while permitting them to rotate freely in their immediate environment. Even a single point of attachment to a cytoplasmic tether would not be likely to inhibit rotational motion completely. The connection is thereby likely to involve several points on extended attachment interfaces. If AChR can also self-aggregate, then cytoplasmic tethers would not be needed on each AChR. Occasional points of anchoring to some AChR molecules might serve to immobilize many AChR.

The interaction between AChR and cytoskeletal elements need not be stable in order to retard rotational motion. If the receptor were rapidly binding and unbinding to an anchoring protein, the slower but nonzero rotational motions observed in both clustered and nonclustered regions could be an average of an immobile and mobile states.

Lipid Specializations

There is evidence from other studies that lipid composition (and perhaps viscosity) in the immediate vicinity of the receptors could be rather specialized. In rat myotubes, cholesterol is present selectively in those areas of AChR clusters that contain the highest AChR concentrations (Pumplin and Bloch, 1983). Numerous other studies have suggested that AChR interacts directly with cholesterol (Middlemas and Raftery, 1987) and that AChR physiological function is affected by membrane cholesterol (Zabrecky and Raftery, 1985; Fong and McNamee, 1987; Criado et al., 1984; Dalziel et al., 1980). Although it seems unlikely that laterally segregated lipid domains would be extensive or viscous enough to account for total immobilization of AChR, such domains may account for some retardation of their rotational diffusion. Further PFRAP experiments with a variety of lipid probes in clustered and nonclustered AChR regions might help elucidate the influence of lipid domains of AChR dynamics.

Effect of Carbachol

Bloch (1986*a*) and Pumplin and Bloch (1987) have shown, and we confirm here by a different assay, that carbachol can disperse clusters. We find, however, that the receptors in clusters that survive a 4–6-h exposure to carbachol remain rotationally immobile ($D_r < 0.2\ s^{-1}$). These surviving clusters appeared relatively intact. It was rare to find bright regions that looked like clusters in the process of dissagregation; but even in such areas, the PFRAP anisotropy remained

high and constant. Although surviving clusters are, by definition, those most immune to carbachol treatment, there is no evidence in Bloch's or our observations that the 4–6-h treatment has reached an endpoint in cluster disaggregation. Therefore, our results suggest that there are no intermediate stages in the mobilization process triggered by carbachol. We see neither the appearance of a time-dependent decay in $r_b(t)$ on the time scale of the experiment (225 ms), nor a decrease in its value that might reflect a higher percentage of rapidly mobile receptors. Evidently, the receptors either are completely released from the cluster, or they remain completely immobilized, preserving their spatial distribution and rotational immobility as clusters. The rupturing effect of carbachol might take place inside the cell, underneath the surviving clusters, but it may be only at the final step of the breakage that the receptors are released from their immediate anchors. Our results are also compatible with carbachol-induced changes in the insertion/degradation rate of the receptor. However, neither Ross et al. (1988) nor Bloch (1986*a*) have found any evidence for this mechanism.

Since the most obvious physiological effect of carbachol on cells is to open AChR ion channels, it is reasonable to hypothesize that the influx of Na^+ ions into the cells under the action of carbachol is responsible for the disaggregation. However, we found that carbachol retained its disaggregating action even on myotubes prelabeled with RBGT, a treatment that should block agonist binding by exposed AChR. Apparently, during the 4–6 h of carbachol treatment after RBGT blockage, some new AChR are incorporated. Indeed, Burszstajn et al. (1985) have measured a significant turnover of receptors in myotube clusters on the 4–6-h time scale. It would be worthwhile to see if continuous exposure to BGT blocks the dissaggregating effect of carbachol.

Effect of Cytochalasin D

We saw no rotational changes in clustered AChR after a 3-h cytochalasin D treatment. Nevertheless, cytochalasin D had a major effect on cell morphology: most cells detached from the substrate during the treatment, and most of the remaining myotubes rounded up into "myoballs" that, however, still retained AChR cluster structures.

Connolly (1984) observed that, in chick myotubes, cytochalasin D induced a partial disappearance of AChR clusters, and suggested that the cytoskeletal disruption could be responsible. Although we did not quantitatively check for partial loss of clusters after cytochalasin treatment on our rat myotubes, we can conclude that AChR rotational immobility is remarkably resilient against major and morphologically obvious disruption of the cytoskeletal structure. Therefore, at least on rat myotubes, AChR anchoring appears to be independent from, or only indirectly related to, the integrity of the nonmyofibrillar actin filaments.

The Technique

PFRAP offers the possibility of measuring rotational motion of proteins on the membrane of living cells, and it is quite practical for measurements of low mobility receptors that are present in medium or high concentrations. The facts that one can use high quantum efficiency fluorophores rather than low quantum efficiency phosphophores, that rather slow rotational motions can be measured, and that sample deoxygenation is not required, are distinct advantages. However, under the worst conditions, measurement of fast rotations of low concentration receptors, many tens of hours of actual data-gathering experimental time may be required to obtain statistically significant $r_b(t)$ curves with the current implementation of PFRAP. But a few improvements should greatly shorten overall experimental time even in the worst conditions. (*a*) A fluorophore that wobbles less at its bond of attachment would increase the expected $r_b(0)$ for "immobile" fluorophore from its present value of $\sim$0.1 toward its theoretical maximum value of 4/7 (Velez and Axelrod, 1988). Just doubling $r_b(0)$, for example, would decrease the experimental time by a factor of four. All present optical techniques for measuring rotational diffusion, including phosphorescence anisotropy, suffer a decrement of signal amplitude due to fast wobbling. A promising approach involves fluorophores that attach to the target protein at two points. (*b*) At least 50% of the experimental time is spent searching manually for the appropriate myotube area in which to collect the data. Therefore, automation of the searching procedure would considerably reduce experimental time. (*c*) The use of a fluorophore with a more homogeneous or predictable reversible recovery behavior at fast time scales would allow us to explore in more detail the rotation of very fast rotating components. (*d*) A fluorophore with a higher emission quantum efficiency would improve the statistical accuracy.

We are indebted to Robert Fulbright for his invaluable help with organosilane chemistry, computer programming, and curve fitting. We also thank Edward Hellen for help with the electronics, Bethe Scalettar of the University of North Carolina for critically reading the manuscript and offering many useful suggestions; Yvette Dorsey, Wei-Ling Ho, Sylvia Shiloff, and Sharada Kumar for preparing the cultures and Laurie Polacek, Electra Coucouvanis, and Andrea Dunathan for general lab support.

This project was supported by: United States Public Health Service (USPHS) grant NS14565 (D. Axelrod); and National Science Foundation grant PCM17271, USPHS grant NS17262, and a Muscular Dystrophy Association of America grant (K. Barald).

Received for publication 27 September 1989 and in revised form 15 February 1990.

References

Anderson, M. J., and M. W. Cohen. 1977. Nerve-induced and spontaneous redistribution of acetylcholine receptors on cultured muscle cells. *J. Physiol. (Lond).* 268;757–773.

Axelrod, D., P. Ravdin, D. E. Koppel, J. Schlessinger, W. W. Webb, E. L. Elson, and T. R. Podleski. 1976. Lateral motion of fluorescently labeled acetylcholine receptors in membranes of developing muscle fibers. *Proc. Natl. Acad. Sci. USA.* 73:4594–4598.

Axelrod, D., P. M. Ravdin, and T. R. Podalski. 1978. Control of acetylcholine receptor mobility and distribution in cultured muscle membranes. A fluorescence study. *Biochim. Biophys. Acta.* 511:23–38.

Barald, K. F., G. D. Phillips, J. C. Jay, and I. F. Mizukami. 1987. A component in mammalian muscle synaptic basal lamina induces clustering of acetylcholine receptors. *Prog. Brain Res.* 71:397–408.

Bartholdi, M., F. J. Barrantes, and T. Jovin. 1981. Rotational molecular dynamics of the membrane-bound acetylcholine receptor revealed by phosphorescence spectroscopy. *Eur. J. Biochem.* 120:389–397.

Bevington, R. B. 1969. Data Reduction and Error Analysis for the Physical Sciences. McGraw-Hill Inc., New York.

Bloch, R. J. 1986*a*. Loss of acetylcholine receptor clusters induced by treatment of cultured rat myotubes with carbachol. *J. Neurosci.* 6:691–700.

Bloch, R. J. 1986*b*. Actin at receptor-rich domains isolated acetylcholine receptor clusters. *J. Cell Biol.* 102:1447–1458.

Bloch, R. J., and Z. W. Hall. 1983. Cytoskeletal components of vertebrate neuromuscular junction: vinculin, alpha-actinin, and filamin. *J. Cell Biol.*

97:217–223.
Bloch, R. J., M. Velez, J. G. Krikorian, and D. Axelrod. 1989. Microfilaments and actin-associated proteins at sites of membrane-substrate attachment within acetylcholine receptor clusters. *Exp. Cell. Res.* 182:583–596.
Brisson, A., and P. N. Unwin. 1985. Quaternary structure of the acetylcholine receptor. *Nature (Lond.).* 315:474–477.
Brown, P. K. 1972. Rhodopsin rotates in the visual receptor membrane. *Nature New Biol.* 236:35–38.
Bursztajn, S., S. A. Berman, J. L. McManaman, and M. L. Watson. 1985. Insertion and internalization of acetylcholine receptors at clustered and diffuse domains on cultured myotubes. *J. Cell Biol.* 101:104–111.
Cherry, R. J. 1979. Rotational and lateral diffusion of membrane proteins. *Biochim. Biophys. Acta.* 559:289–327.
Cone, R. A. 1972. Rotational and lateral diffusion of rhodopsin in the visual receptor membrane. *Nature New Biol.* 236:39–43.
Connolly, J. A. 1984. Role of the cytoskeleton in the formation, stabilization, and removal of acetylcholine receptor clusters in cultured muscle cells. *J. Cell Biol.* 99:148–154.
Connolly, J. A., and A. J. Graham. 1985. Actin filaments and acetylcholine receptor clusters in embryonic chick myotubes. *Eur. J. Cell Biol.* 37:191–195.
Criado, M., H. Eibl, and F. J. Barrantes. 1984. Functional properties of the acetylcholine receptor incorporated in model lipid membranes. Differential effects of chain length and head group of phospholipids on receptor affinity states and receptor mediated ion translocation. *J. Biol. Chem.* 259:9188–9198.
Dalziel, A. W., E. S. Rollins, and M. G. McNamee. 1980. The effect of cholesterol on agonist-induced flux in reconstituted acetylcholine receptor vesicles. *FEBS (Fed. Eur. Biochem. Soc.) Lett.* 122:193–196.
Edidin, M. 1987. Rotational and lateral diffusion of membrane proteins and lipids phenomena and function. *Curr. Topics Membr. Trans.* 29:91–127.
Englander, L., and L. L. Rubin. 1987. Acetylcholine receptor clustering and nuclear movement in muscle fibers in culture. *J. Cell Biol.* 104:87–95.
Fong, T. M., and M. G. McNamee. 1987. Stabilization of acetylcholine receptor structure by cholesterol and negatively charged phospholipids in membranes. *Biochemistry.* 26:3871–3889.
Frank, E., and G. D. Fishbach. 1979. Early events in neuromuscular junction formation in vitro. Induction of acetylcholine receptor clusters in the postsynaptic membrane and morphology of newly formed nerve-muscle synapses. *J. Cell Biol.* 83:143–158.
Gonzalez-Rodriguez, J., and A. U. Acuna. 1987. Probing molecular dynamics of proteins in biological membranes by optical spectroscopy: rotational diffusion. *Revis Biol. Celular.* 11:47–74.
Harris, D. A., D. L. Falls, and G. D. Fishbach. 1989. Differential activation of myotube nuclei following exposure to an acetylcholine receptor inducing factor. *Nature (Lond.).* 337:173–176.
Heuser, J. E., and S. R. Saltpeter. 1979. Organization of acetylcholine receptors in quick-frozen, deep-etched, and rotary-replicated *Torpedo* postsynaptic membrane. *J. Cell Biol.* 82:150–173.
Hirokawa, N., and J. E. Heuser. 1982. Internal and external differentiations of the postsynaptic membrane at the neuromuscular junction. *J. Neurocytol.* 11:487–510.
Jacobson, B. S., J. Cronin, D. Branton. 1978. Coupling polylysine to glass beads for plasma membrane isolation. *Biochim. Biophys. Acta.* 506:81–96.
Jacobson, K., A. Ishihara, and R. Inman. 1987. Lateral diffusion of proteins in membranes. *Annu. Rev. Physiol.* 49:163–175.
Johnson, P., and P. B. Garland. 1982. Fluorescent triplet probes for measuring the rotational diffusion of membrane proteins. *Biochem. J.* 203:313–321.
Koppel, D. E., M. P. Sheetz, and M. Schindler. 1981. Matrix control of protein diffusion in biological membranes. *Proc. Natl. Acad. Sci. USA.* 78:3576–3580.
Kuromi, H. 1987. Mechanism of acetylcholine receptor accumulation at the nerve-muscle junction during development. *Asia Pac. J. Pharmacol.* 2: 195–202.
Lo, M. M. S., P. B. Garland, J. Lamprecht, and E. A. Barnard. 1980. Rotational mobility of the membrane-bound acetylcholine receptor of Torpedo electric organ measured by phosphorescence depolarization. *FEBS (Fed. Eur. Biochem. Soc.) Lett.* 111:407–412.
Middlemas, D. S., and M. A. Raftery. 1987. Identification of subunits of acetylcholine receptor that interact with a cholesterol photoaffinity probe. *Biochemistry.* 26:1219–1223.
Nigg, E. A., and R. J. Cherry. 1980. Anchorage of a band 3 population at the erythrocyte cytoplasmic membrane surface. Protein rotational diffusion measurements. *Proc. Natl. Acad. Sci. USA.* 77:4702–4706.
Olek, A. J., J. G. Krikorian, and M. P. Daniels. 1986. Early stages in the formation and stabilization of acetylcholine receptor aggregates on cultured myotubes: sensitivity to temperature and azide. *Dev. Biol.* 117:24–34.
Pavlath, G. K., K. Rich, S. G. Webster, and H. M. Blau, 1989. Localization of muscle gene products in nuclear domains. *Nature (Lond.).* 337:570–573.
Peng, H. B. 1983. Cytoskeletal organization of the presynaptic nerve terminal and the acetylcholine receptor cluster in cell cultures. *J. Cell Biol.* 97: 489–498.
Peng, H. B., and S. C. Froehner. 1985. Association of the postsynaptic 43K protein with newly formed acetylcholine receptor clusters in cultured muscle cells. *J. Cell Biol.* 99:344–349.
Peng, H. B., and M. Poo. 1986. Formation and dispersal of acetylcholine receptors in cultured muscle cells. *Trends Neurosci.* 9:125–129.
Peng, H. B., D. Y. Zhao, M. Z. Xie, Z. W. Shen, and K. Jacobson. 1989. The role of lateral migration in the formation of acetylcholine receptor clusters induced by basic polypeptide-coated latex beads. *Dev. Biol.* 131:197–206.
Peters, R., and R. J. Cherry. 1982. Lateral and rotational diffusion of bacteriorhodopsin in lipid bilayers: experimental test of the Saffman-Delbruck equations. *Proc. Natl. Acad. Sci. USA.* 79:4317–4321.
Peterson, O. N. 1984. Diffusion and aggregation in biological membranes. *Can. J. Biochem. Cell Biol.* 62;1158–1166.
Pumplin, D. W., and R. Bloch. 1983. Lipid domains of acetylcholine receptor clusters detected with saponin and filipin. *J. Cell Biol.* 97:1043–1054.
Pumplin, D. W., and R. J. Bloch. 1987. Disruption and reformation of acetylcholine receptor clusters of cultured rat myotubes occur in two distinct stages. *J. Cell Biol.* 104:97–108.
Richter, C., K. H. Winterhalter, and R. J. Cherry. 1979. Rotational diffusion of cytochrome P-450 in rat liver microsomes. *FEBS (Fed. Eur. Biochem. Soc.) Lett.* 102:151–154.
Ross, A., M. Rapuano, and J. Prives. 1988. Induction of phosphorylation and cell surface redistribution of acetylcholine receptors by phorbol ester and carbamylcholine in cultured chick muscle cells. *J. Cell Biol.* 107:1139–1145.
Rousselet, A., J. Cartaud, P. F. Devaux, and J.-P. Changeux. 1982. The rotational diffusion of the acetylcholine receptor in Torpedo marmorata membrane fragments studied with a spin-labeled a-toxin: importance of the 43,000 protein(s). *EMBO (Eur. Mol. Biol. Organ.) J.* 1:439–445.
Saffman, P. G., and M. Delbruck. 1975. Brownian motion in biological membranes. *Proc. Natl. Acad. Sci. USA.* 72:3111–3113.
Scalettar, B., P. Selvin, D. Axelrod, J. E. Hearst, and M. P. Klein. 1990. Rotational diffusion of DNA in agarose gels. *Biochemistry.* In press.
Schlessinger, J. 1983. Mobilities of cell-membrane proteins: how are they modulated by the cytoskeleton. *Trends Neurosci.* 6:360–363.
Schuetze, S. M., and L. W. Role. 1987. Developmental regulation of nicotinic acetylcholine receptors. *Annu. Rev. Neurosci.* 10:403–457.
Sealock, R., B. E. Wray, and S. C. Froehner. 1984. Talin is a component of the rat neuromuscular junction. *Exp. Cell Res.* 163:143–150.
Stollberg, J., and S. E. Fraser. 1988. Acetylcholine receptors and concanavalin A-binding sites on cultured Xenopus muscle cells: electrophoresis, diffusion and aggregation. *J. Cell Biol.* 107:1397–1408.
Stya, M., and D. Axelrod. 1983. Diffusely distributed acetylcholine receptors can participate in cluster formation on cultured rat myotubes. *Proc. Natl. Acad. Sci. USA.* 80:449–453.
Velez, M., and D. Axelrod. 1988. Polarized fluorescence photobleaching recovery for measuring rotational diffusion in solutions and membranes. *Biophys. J.* 53:575–591.
Wolf, D. E. 1986. Probing the lateral organization and dynamics of membranes. *In* Spectroscopic Membrane Probes. Vol. I. CRC Press, Boca Raton. 193–219.
Yoshida, T. M., and B. G. Barisas. 1986. Protein rotational motion in solution measured by polarized fluorescence depletion. *Biophys. J.* 50:41–53.
Zabrecky, J. R., and M. A. Raftery. 1985. The role of lipids in the function of the acetylcholine receptor. *J. Recept. Res.* 5:397–417.
Zidovetski, R., J. Yarden, J. Schlesinger, and T. M. Jovin. 1981. Rotational diffusion of epidermal growth factor complexed to cell surface receptors reflects rapid microaggregation and endocytosis of occupied receptors. *Proc. Natl. Acad. Sci. USA.* 78:6981–6985.